Territories of heterologous inputs onto Purkinje cell dendrites are segregated by mGluR1-dependent parallel fiber synapse elimination

Ryoichi Ichikawa[a,1], Kouichi Hashimoto[b], Taisuke Miyazaki[c], Motokazu Uchigashima[c], Miwako Yamasaki[c], Atsu Aiba[d], Masanobu Kano[e], and Masahiko Watanabe[c,1]

[a]Department of Anatomy, Sapporo Medical University School of Medicine, Sapporo 060-8556, Japan; [b]Department of Neurophysiology, Graduate School of Biomedical & Health Sciences, Hiroshima University, Hiroshima 734-8551, Japan; [c]Department of Anatomy, Hokkaido University Graduate School of Medicine, Sapporo 060-8638, Japan; [d]Laboratory of Animal Resources, Center for Disease Biology and Integrative Medicine, Faculty of Medicine, University of Tokyo, Bunkyo-ku, Tokyo 113-0033, Japan; and [e]Department of Neurophysiology, Graduate School of Medicine, University of Tokyo, Tokyo 113-0033, Japan

Edited by Jeff W. Lichtman, Harvard University, Cambridge, MA, and approved January 14, 2016 (received for review June 12, 2015)

In Purkinje cells (PCs) of the cerebellum, a single "winner" climbing fiber (CF) monopolizes proximal dendrites, whereas hundreds of thousands of parallel fibers (PFs) innervate distal dendrites, and both CF and PF inputs innervate a narrow intermediate domain. It is unclear how this segregated CF and PF innervation is established on PC dendrites. Through reconstruction of dendritic innervation by serial electron microscopy, we show that from postnatal day 9–15 in mice, both CF and PF innervation territories vigorously expand because of an enlargement of the region of overlapping innervation. From postnatal day 15 onwards, segregation of these territories occurs with robust shortening of the overlapping proximal region. Thus, innervation territories by the heterologous inputs are refined during the early postnatal period. Intriguingly, this transition is arrested in mutant mice lacking the type 1 metabotropic glutamate receptor (mGluR1) or protein kinase Cγ (PKCγ), resulting in the persistence of an abnormally expanded overlapping region. This arrested territory refinement is rescued by lentivirus-mediated expression of mGluR1α into mGluR1-deficient PCs. At the proximal dendrite of rescued PCs, PF synapses are eliminated and free spines emerge instead, whereas the number and density of CF synapses are unchanged. Because the mGluR1-PKCγ signaling pathway is also essential for the late-phase of CF synapse elimination, this signaling pathway promotes the two key features of excitatory synaptic wiring in PCs, namely CF monoinnervation by eliminating redundant CF synapses from the soma, and segregated territories of CF and PF innervation by eliminating competing PF synapses from proximal dendrites.

cerebellum | Purkinje cell | climbing fiber | parallel fiber synapse elimination

Monoinnervation of cerebellar Purkinje cells (PCs) by single climbing fibers (CFs) is established in the early postnatal period (1–3). The soma of a neonatal PC is innervated by more than five CFs with similar synaptic strengths, from which a single CF is functionally strengthened (4, 5). The strengthened ("winner") CF starts dendritic translocation, whereas the other weaker ("loser") CFs remaining on the soma are eliminated (6–8). In this process, P/Q-type voltage-dependent Ca^{2+} channels (VDCCs) promote functional differentiation and dendritic translocation of winner CFs, and the early phase of CF synapse elimination (9–11), whereas the late phase of CF synapse elimination is critically dependent on the formation of parallel fiber (PF) synapses and activation of the type 1 metabotropic glutamate receptor (mGluR1)-protein kinase Cγ (PKCγ) pathway (12–17).

Segregated dendritic innervation by CFs and PFs is another distinguished feature of the PC synaptic wiring. Although hundreds of thousands of PFs innervate the distal dendritic domain, a single CF monopolizes the proximal dendritic domain, and both innervate a narrow intermediate domain (18). Given that both dendritic translocation of winner CFs and formation of PF synapses proceed upwards from the base of the dendritic tree (6, 19), CFs and PFs must compete with each other to establish their segregated territories. However, the developmental route and the underlying mechanisms of this process are unknown.

Our findings indicate that CF and PF territories on PC dendrites are dynamically refined during the early postnatal period, and that the mGluR1-PKCγ signaling pathway regulates segregation by promoting PF synapse elimination. Thus, this signaling cascade plays key roles in sculpting the excitatory synaptic wiring in PCs by eliminating both redundant CF synapses from the soma (3, 20) and competing PF synapses from the proximal dendrites.

Results

CF and PF Projection onto PCs. We examined development of CF and PF projections onto PCs by triple fluorescent labeling. Calbindin immunofluorescence showed that PC dendrites were short and immature at P7; they were progressively elongated and branched thereafter, and established well-arborized dendritic trees at postnatal day (P) 30 (Fig. 1 *A–F*, green). Tracer labeling with biotinylated dextran amine (BDA) injected into the inferior olive (*SI Materials and Methods*) revealed that CF innervation was confined to PC somata at P7, commenced dendritic translocation at P9, and extended thereafter (Fig. 1 *A–F*, red). The mean heights of PC dendrites and CFs continued to increase from P7 to P30 (Fig. 1*G*), with the latter attaining >80% of the molecular layer thickness at P20 and P30 (Fig. 1*H*). Vesicular glutamate transporter 1 (VGluT1), which replaces VGluT2 in maturating terminals along T-shaped granule cell axons (21), was distributed on the basal side of the molecular layer from P7 to

Significance

Of the two distinguished features in synaptic wiring of cerebellar Purkinje cells (PCs), the developmental process and underlying mechanism of mono-innervation by single climbing fibers (CFs) are well understood. However, those of segregated dendritic innervation by CFs and parallel fibers (PFs) remain unknown. Here, we show that CF and PF territories initially expand with enlargement of the region of overlapping innervation, and that the segregation of the territories occurs as a result of elimination of PF synapses from the proximal dendrites. PF synapse elimination is controlled by the type 1 metabotropic glutamate receptor (mGluR1) to protein kinase Cγ signaling pathway; PF synapse elimination is arrested in mGluR1- or protein kinase Cγ-knockout PCs, and rescued by mGluR1α transfection to mGluR1-knockout PCs.

Author contributions: R.I. and M.W. designed research; R.I., K.H., T.M., and M.U. performed research; M.Y., A.A., and M.W. contributed new reagents/analytic tools; R.I. and K.H. analyzed data; and R.I., K.H., M.K., and M.W. wrote the paper.

The authors declare no conflict of interest.

This article is a PNAS Direct Submission.

[1]To whom correspondence may be addressed. Email: richi@sapmed.ac.jp or watamasa@med.hokudai.ac.jp.

This article contains supporting information online at www.pnas.org/lookup/suppl/doi:10.1073/pnas.1511513113/-/DCSupplemental.

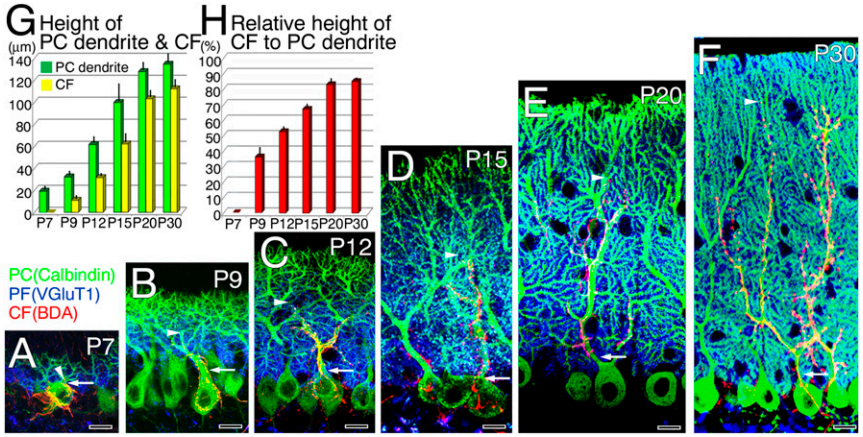

Fig. 1. Development of CF and PF projections onto PC dendrites in postnatal mouse cerebella. (*A*–*F*) Triple fluorescent labeling for CFs (red, BDA tracer labeling), PF terminals (blue, VGluT1 immunofluorescence), and PCs (green, calbindin immunofluorescence) at P7 (*A*), P9 (*B*), P12 (*C*), P15 (*D*), P20 (*E*), and P30 (*F*). Arrowheads indicate the tip of the CF projection, and arrows indicate the somatodendritic border of PCs. (Scale bars, 10 μm.) (*G*) The mean vertical height (μm, mean ± SD, $n = 3$ mice at each stage) to the tips of PC dendrites (green) or CFs (yellow). To evaluate the vertical height, 10 PC dendrites and 10 CFs were analyzed in each mouse. (*H*) The vertical height of the CF projection relative to that of PC dendrites (%, mean ± SD, $n = 3$ mice at each stage).

P20, and fully filled the layer at P30 (Fig. 1 *A*–*F*, blue). Thus, dendritic differentiation of PCs, dendritic translocation of CFs, and neurochemical maturation of granule cell axons including PFs proceed together and are completed at P30.

Reconstruction of Dendritic Innervation. Next, we examined dendritic innervation. At each stage we sampled three PCs in which BDA-labeled CFs could be accurately traced in single sections from the base of PC somata to the tips of CFs (Fig. S1 *A*–*F*). The sections were processed for 3,3′-diaminobenzidine precipitate labeling for BDA and metal particle labeling for VGluT1, and then subjected to serial electron microscopic pursuit along single dendritic tracks (Fig. S1 *G*–*X*).

All of the BDA-labeled CF terminals (Fig. S2*A*) and the VGluT1-labeled PF terminals (Fig. S2*B*) formed asymmetrical synapses on dendritic spines. Symmetrical synapses were usually formed on dendritic shafts of PCs and labeled for vesicular inhibitory amino acid transporter VIAAT (Fig. S2*C*) (i.e., GABAergic synapses from molecular layer interneurons). At some developmental stages, we also encountered VIAAT-labeled symmetrical synapses on PC spines (Fig. S2 *D* and *E*) and free spines lacking synaptic contact (Fig. S2*F*). The three spine-type synapses and free spines are reconstructed in Fig. 2 and Fig. S3, where CF synapses (yellow circles on red lines) and PF synapses (blue circles) are plotted to the right of each dendrite, whereas atypical GABAergic synapses on spines (green circles) and free spines (black squares) are to the left. From these reconstructed data, we quantitatively analyzed the territories and patterns of innervation by CFs and PFs and the distribution of free spines.

Refinement of CF and PF Territories. Three domains of PC dendrites were defined based on the synaptic inputs as determined by serial electron microscopy: PC dendrite-I (PCD-I), innervated by CFs alone (Fig. 3*A*, orange), PCD-II, innervated by both CFs and PFs (Fig. 3*A*, pink), and PCD-III, innervated by PFs alone (Fig. 3*A*, blue). Because reconstructed dendrites were usually curved or leaning in serial sections, we calculated the path length of dendrites in serial sections using the long and short diameters of dendritic profiles and the thickness and the number of sections (Fig. S4).

At P7, PC dendrites were innervated by PFs only, whereas CF innervation was confined to the soma of PCs (Fig. 3*A*). At P9 and thereafter, PCD-I and PCD-II domains appeared and elongated, reflecting dendritic translocation of CFs. The mean path length of the CF territory—that is, the combined length of the PCD-I and PCD-II domains—increased progressively from P9 to P30 (Fig. 3*B*, yellow columns). This increase was attributed to an initial expansion of the PCD-II domain (up to P15) and the subsequent elongation of the PCD-I domain (P15 onwards) (Fig. 3*A*). In comparison, the mean path length of the PF territory (i.e., summed length of the PCD-II and PCD-III domains) markedly increased from P7 to P15, but decreased thereafter (Fig. 3*B*, blue columns). Because the path length of the PCD-III domain was fairly constant in the postnatal period examined, the change in PF territory is primarily attributed to initial elongation (up to P15) and subsequent constriction (P15 onwards) of the PCD-II domain (Fig. 3*A*). Therefore, CF and PF territories grow vigorously until P15, with expansion of their overlapping PCD-II domain; after P15 they segregate by replacing the PCD-II domain with the PCD-I domain. In parallel with the territory refinement, spines were apparently reduced at proximal dendrites between P15 and P20, as visualized by lentivirus-mediated labeling of single PCs with GFP (Fig. 3 *C*–*F*), suggesting active synaptic reorganization at proximal dendrites.

Refinement of CF and PF Synapses and Free Spines. We also analyzed changes in dendritic innervation by CF and PF synapses. The mean number of CF synapses per analyzed dendritic track displayed an initial steep increase until P15, a transient decrease at P20, and a second modest increase at P30 (Fig. 3*G*, yellow columns). The

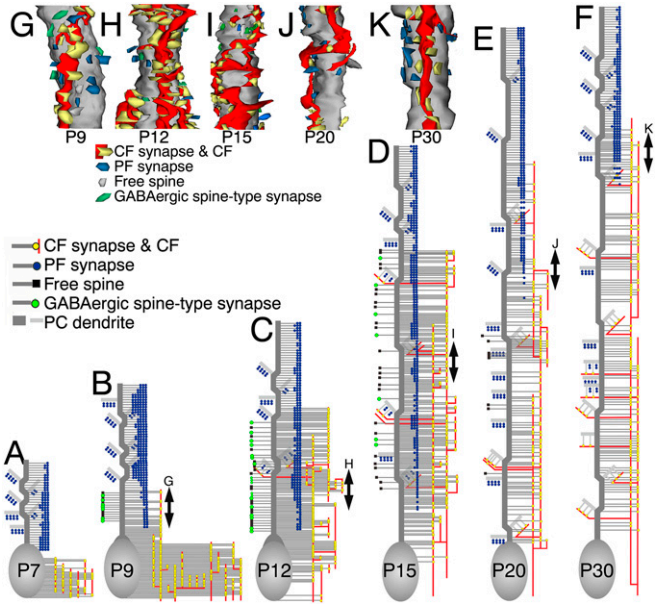

Fig. 2. Reconstructed dendritic innervation in wild-type PCs at P7 (*A*), P9 (*B* and *G*), P12 (*C* and *H*), P15 (*D* and *I*), P20 (*E* and *J*), and P30 (*F* and *K*). (*A*–*F*) CF synapses (yellow circles on red lines) and PF synapses (blue circle) are shown to the right of PC somata and dendrites (gray), whereas GABAergic spine-type synapses (green circle) and free spines (black square) are to the left of dendrites. One of the three PCs examined at each stage is illustrated here, with the rest being shown in Fig. S3. (*G*–*K*) Three-dimensional reconstructed images of dendritic innervation. Dendritic portions of double-headed arrows in *B*–*F* are illustrated.

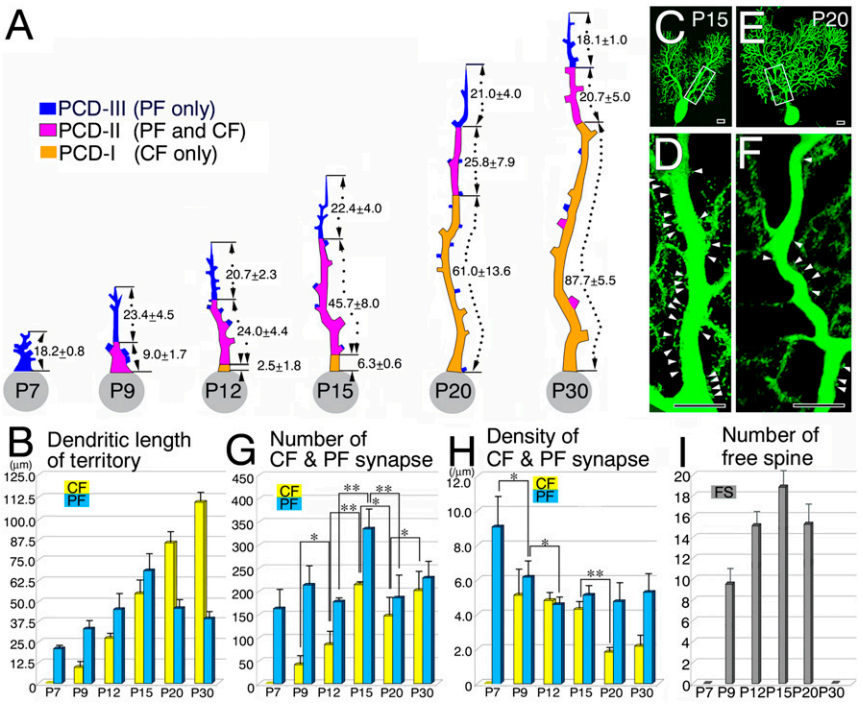

Fig. 3. Developmental changes in territories and patterns of CF and PF innervation on PC dendrites. (*A*) Schematic drawings showing the mean path length of the three dendritic domains at P7–P30 (μm, mean ± SD). Shown are the CF-dominant PCD-I (orange), the overlapping PCD-II (pink), and the PF-dominant PCD-III (blue) domains. (*B*) The mean path length of CF territories (yellow columns) and PF territories (blue columns) (μm, mean ± SD, $n = 3$ dendrites each). From P15 onwards, the CF territory elongates, whereas the PF territory is reciprocally shortened. (*C*–*F*) Lentivirus-mediated GFP labeling of PCs at P15 (*C* and *D*) and P20 (*E* and *F*). Boxed regions in *C* and *E* are enlarged in *D* and *F*, respectively. Arrowheads indicate spiny protrusions from proximal shaft dendrites. (Scale bars, 5 μm.) (*G*) The mean number of CF (yellow bars) and PF (blue bars) synapses per analyzed dendritic track (mean ± SD, $n = 3$ dendrites at each stage). (*H*) The mean density of CF synapses in the CF territory (yellow bars) and PF synapses in the PF territory (blue bars) (mean ± SD, $n = 3$). Synapse density is indicated per 1 μm of dendritic path length. (*I*) The mean number of free spines per analyzed dendritic track ($n = 3$, mean ± SD). The *P* value was calculated using Student's *t* test. $*P < 0.05$; $**P < 0.01$.

density of CF synapses in the CF territory was high in P9–P15, and decreased to less than half of this level at P20 and P30 (Fig. 3*H*, yellow columns). These results suggest that the initial increase in CF synapse number is achieved by high-density synaptogenesis on an expanding CF territory. It is likely that the subsequent drop in CF synapse number at P20 is caused by a marked decrease in synapse density, and the recovery at P30 is caused by further expansion of the CF territory.

Postnatal changes in the mean number of PF synapses were generally similar to those of CF synapses (Fig. 3*G*, blue columns). Of note, after peaking at P15, the number of PF synapses per analyzed dendritic track decreased at P20 and P30 to nearly half of the peak level. In contrast, the density of PF synapses in the PF territory was constant after P12, following a marked reduction from P7 to P12 (Fig. 3*H*, blue columns). The reduction in PF synapse number at P20 and P30 is thereby a result of contraction of the PF territory. Therefore, the major change of dendritic innervation from P15 to P20 (or P30) is that the density of CF synapses is reduced on the expanding CF territory, whereas the density of PF synapses is maintained on the contracting PF territory, resulting in marked numerical loss of PF synapses.

Free spines appeared at P9, peaked at P15, and disappeared by P30 (Fig. 3*I*). They were distributed in the CF territory, never in the PCD-III (Fig. 2 *B*–*D* and Fig. S3 *B*–*D*). Thus, free spines are transient structures during active refinement in dendritic innervation by CFs and PFs.

Refinement of Functional PF Synapses. The postnatal rearrangement of PF and CF synapses could affect the distribution of functional synapses on PC dendrites. To test this possibility, we recorded miniature excitatory postsynaptic currents (mEPSCs) from PCs in cerebellar slices from mice at P14–P20 (*SI Materials and Methods* and Fig. S5*A*). We estimated the location of functional synapses on PC dendrites from the 10–90% rise times of mEPSCs (6). We found that frequency distribution histograms for the 10–90% rise time were similar for P14–P16 and for P18–P20 except several time points (Fig. S5*B*). In particular, the incidence of mEPSCs with rise times of 0.2–0.6 ms was significantly higher at P14–P16 than at P18–P20 (Fig. S5*C*). These mEPSCs with fast rise times are considered to be elicited at proximal parts of PC dendrites, because the majority of quantal EPSCs arising from CF synapses on proximal dendrites had rise times faster than 1 ms (Fig. S5*D*) (6, 17, 22). To determine the origin of the mEPSCs with fast rise time, we used L-AP4 (50 μM), a blocker of group III mGluRs that selectively suppresses PF synaptic transmission without an appreciable effect on CF synaptic transmission (22, 23). We found that the frequency of the mEPSCs with rise

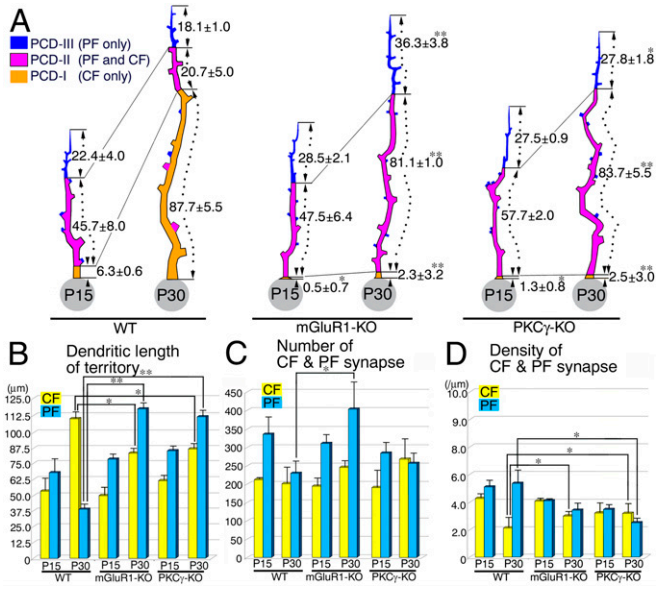

Fig. 4. Arrested refinement of CF and PF innervation in mGluR1-KO and PKCγ-KO mice. (*A*) Schematic drawings showing the mean path length of three dendritic domains (μm, mean ± SD). See legend in Fig. 3*A*. (*B*) The mean path length of CF and PF territories. Note a marked shortening of the CF territory with a reciprocal elongation of the PF territory in both mutants at P30. (*C* and *D*) The mean number (*C*) and density (*D*) of CF (yellow columns) and PF (blue columns) synapses (mean ± SD, $n = 3$ dendrites at each stage). Data from wild-type mice at P15 and P30 are reproduced from Fig. 3*A*. Statistical differences between mutant and wild-type mice are indicated with asterisks ($*P < 0.05$; $**P < 0.01$).

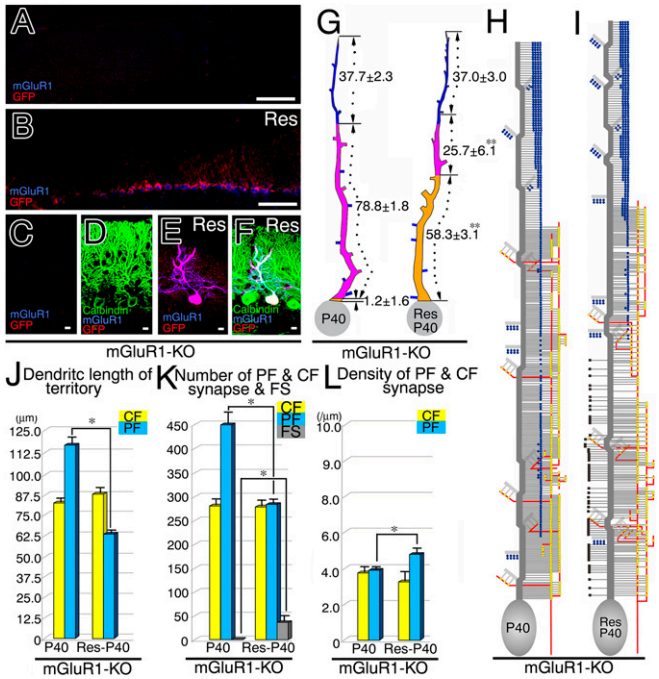

Fig. 5. Restored refinement in CF and PF innervation after lentiviral transfection of mGluR1α in mGluR1-KO PCs. (*A–F*) Triple fluorescent labeling for GFP (red), mGluR1α (blue), and calbindin (green) in mGluR1α/GFP-transfected mGluR1-KO cerebellum at P40. Untransfected (*A*, *C*, and *D*) and transfected (*B*, *E*, and *F*) cerebellar portions are shown. (*G* and *H*) Reconstructed dendritic innervation in mGluR1-KO (*G*) and rescued (*H*) PCs. One of the three PCs examined in mGluR1-KO and mGluR1α-rescued PCs is illustrated here, with the rest being shown in Fig. S7. (*I*) The mean path lengths of the three dendritic domains (μm, mean ± SD). (*J–L*) Bar graphs showing the mean path lengths of CF and PF territories (*J*), the mean number of CF synapses, PF synapses, and free spines (*K*), and the mean density of CF and PF synapses (*L*). Note the emergence of free spines in the CF territory of rescued PCs (black squares in *H* and gray column in *K*). See legends for Figs. 2 and 3. (Scale bars, 100 μm in *A* and *B;* 10 μm in *C–F*.)

time of 0.2–0.6 ms was suppressed by bath-applied L-AP4 at P14–P15 but not at P18–P20 (Fig. S5*E*). Because quantal CF-EPSC was insensitive to L-AP4 (Fig. S5*F*), the component of mEPSCs suppressed by L-AP4 was judged to arise from PF synapses. This PF-mediated component was relatively small because of the significant contribution of L-AP4–insensitive CF-mediated component in mEPSCs with fast rise times. However, these findings show the presence of PF-mediated mEPSCs in dendrites with the same electrotonic distance from the soma as CF-mediated ones. Taken together, the results suggest that the PF synapses present transiently on proximal dendrites are functional and that they decrease from P14–P16 to P18–P20.

Arrested Refinement in mGluR1-KO and PKCγ-KO Mice. The late phase of CF synapse elimination is critically dependent on the mGluR1-to-PKCγ signaling cascade (12–17). Temporal coincidence of the territory refinement with the late phase of CF synapse elimination prompted us to test possible involvement of this signaling cascade in the territorial segregation. We thus reconstructed CF and PF innervation patterns in mGluR1-knockout (KO) and PKCγ-KO mice at P15 and P30 by serial electron microscopy (Fig. S6).

At P15, no significant abnormalities were noted in both mutants, in terms of the composition of dendritic domains (Fig. 4*A* and Fig. S6 *E* and *G*), path length of CF and PF territories (Fig. 4*B*), and the number and density of CF and PF synapses (Fig. 4 *C* and *D*). Significant differences became apparent in most parameters in these mutant mice at P30, compared with those in wild-type mice at P30. Notably, the PF territory continued to expand downward to the somatodendritic border in both mutants (Fig. 4*A* and Fig. S6 *F* and *H*), resulting in marked elongation of the PF territory (Fig. 4*B*). Concomitantly, the CF territory was contracted (Fig. 4*B*), with increased densities of CF synapses in both mutants at P30 (Fig. 4*D*). Because these phenotypes are essentially the same as those observed in wild-type mice at P15, genetic ablation of mGluR1 or PKCγ is considered to arrest the developmental refinement of CF and PF innervation.

Restored Refinement by mGluR1α Transfection into mGluR1-KO PCs. Finally, we examined whether PC-specific expression of mGluR1α rescued the phenotypes of mGluR1-KO mice. We injected lentiviral vector into the mGluR1-KO cerebella at P20 for the expression of mGluR1α and GFP under the control of the PC-specific *L7* promoter (24, 25) (*SI Materials and Methods*). At P40, we confirmed the expression of mGluR1α and GFP in a subset of calbindin-positive PCs (Fig. 5 *A–F*). Immunofluorescent signals for transfected mGluR1α in mGluR1-KO PCs appeared less intense than those for native mGluR1α in wild-type PCs. We sampled three mGluR1$^+$ (rescued) and three mGluR1$^-$ (mGluR1-KO) PCs to reconstruct their dendritic innervation by CFs and PFs (Fig. 5 *G–I* and Fig. S7).

mGluR1-KO PCs at P40 were almost comparable to those at P30, in terms of virtual lack of the PCD-I domain (Fig. 5*G*), elongated PF territory (Fig. 5*J*), and increased number of PF synapses (Fig. 5*K*). In contrast, rescued PCs displayed marked elongation of the PCD-I domain and reciprocal shortening of the PCD-II domain (Fig. 5*G*), leading to significant contraction of the PF territory (Fig. 5*J*). Furthermore, the mean number of PF synapses was reduced but their density was slightly increased in mGluR1-rescued PCs (Fig. 5 *K* and *L*). Transfection of mGluR1α thus restores the normal development of CF and PF innervation. Notably, free spines emerged in the CF territory of rescued PCs (Fig. 5*I* and Fig. S7*B*), with no apparent changes in CF synapse number and density (Fig. 5 *K* and *L*), suggesting that free spines are produced by mGluR1α-mediated PF synapse elimination at proximal dendrites.

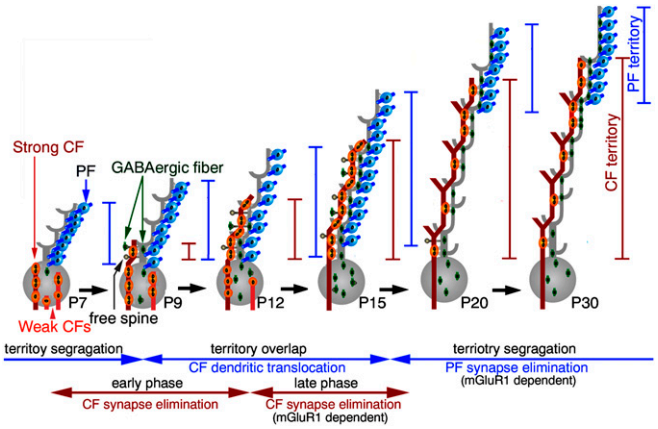

Fig. 6. Territory refinement by CF and PF innervation in PCs. In the territory overlap phase (P9–P15), a winner CF (red) translocates to PC dendrites, weaker CFs (pink) remain on the soma, and newly differentiated PF synapses (blue) are added on to the growing tips of dendritic trees. All of these events fuel synaptic competitions among homologous and heterologous inputs, but their territories of innervation do not remain segregated. In the territory segregation phase (P15 onward), PF synapses are eliminated from overlapping dendritic portions, leading to the segregation of the CF and PF territories. Moreover, redundant CF synapses remaining on PC somata are eliminated, establishing CF mono-innervation. The mGluR1 signaling pathway promotes both the elimination of CF synapses from the soma (the late phase of CF synapse elimination, P12–P17) and the elimination of PF synapses from proximal dendrites. As a result, redundant innervations by homologous and heterologous inputs are refined into input-selective wiring in PCs (i.e., CF monoinnervation and segregated territories of CF and PF innervation).

Discussion

The present study has demonstrated that dendritic innervation by CFs and PFs proceeds in two distinct phases, and that the phase transition requires mGluR1-PKCγ signaling.

Territory Overlap and Segregation Phases. CF and PF territories are initially separated at P7, the former being on the PC soma and the latter on the dendrite, and then they overlap from P9 to P15 (Fig. 6). In this territory overlap phase, a single winner CF starts dendritic translocation from P9 onwards, whereas the other loser CFs remain on the soma until being eliminated by P15–P17 (4, 6, 7). It is also during this phase that PF synapses are massively generated (19), and the source of somatic innervation switches from glutamatergic CF synapses to GABAergic basket cell synapses (7), both of which are essential to establish CF monoinnervation (2, 3, 6, 26). Thus, the territory overlap phase temporally coincides with active stages of homosynaptic competition among CFs, and heterosynaptic competitions between CFs and PFs or basket cell axons.

From P15 onwards, CF and PF territories are resegregated by marked elongation of the PCD-I domain and reciprocal shortening of the PCD-II domain (Fig. 6). Territory segregation from P15 is thus achieved by elimination of PF synapses at the PCD-II domain, reforming it into the PCD-I domain, rather than by membrane expansion of the PCD-I domain itself. Taken together, the territory overlap and the subsequent segregation are driven by dendritic translocation of single winner CFs and elimination of PF synapses from the overlapping portions, respectively. The PF synapse elimination is further supported by our electrophysiological finding that the incidence of mEPSCs with fast rise times decreased from P14–P16 to P18–P20.

mGluR1-Mediated Synapse Elimination. Comparable innervation patterns between wild-type and mGluR1-KO or PKCγ-KO PCs at P15 indicate that overlapping innervation develops independently of mGluR1 signaling. The ablation of mGluR1 or PKCγ selectively impaired a developmental transition to the territory segregation phase, and consequently, PF synapses continued to cover almost all dendritic trees at P30 and P40. Furthermore, arrested refinement in mGluR1-KO mice was rescued by mGluR1α expression in PCs. These findings suggest that the mGluR1 signaling pathway promotes the elimination of PF synapses at proximal dendrites. Considering its essential role in CF synapse elimination (3, 20), the mGluR1-PKCγ signaling pathway has a dual function in excitatory synaptic wiring on to PCs, namely CF synapse elimination from the soma and PF synapse elimination from proximal dendrites.

In PCs, mGluR1 is readily activated by PF stimulation and induces inositol 1,4,5-trisphosphate–mediated Ca^{2+} release from internal Ca^{2+} stores in local dendritic regions (27, 28). Furthermore, mGluR1 can also be activated by CF stimulation (29, 30). Hence, activities along PF and CF afferents likely drive mGluR1-PKCγ signaling in PCs and eliminate redundant CF and PF synapses.

Factors Regulating Segregated Dendritic Innervation. P/Q-type VDCCs are activated upon CF firing and mediate global Ca^{2+} influx in the whole dendritic tree (31–33). P/Q-type VDCC-KO mice exhibit more severe defects in CF synapse development than mutant mice deficient in the mGluR1 signaling pathway. P/Q-type VDCC-KO mice are impaired in selective functional strengthening and dendritic translocation of single winner CFs, resulting in a diminished territory by winner CFs and abnormal persistence of weaker CFs and PFs in the same somatodendritic compartment (9–11). Therefore, local and global Ca^{2+} dynamics, which are mediated by the mGluR1 signaling pathway and P/Q-type VDCCs, respectively, may work in concert to drive CF synapse elimination from the soma and PF synapse elimination from proximal dendrites. Through these mechanisms, single winner CFs can elongate their innervation territories by eliminating competing weaker inputs.

PF synapses are endowed with a specific synaptic adhesion system mediated by GluD2, Cbln1, and neurexin (34, 35). GluD2-KO mice exhibit a severe loss of the PCD-III domain, and aberrantly extended CF territory toward the tip of the PC dendritic tree (18). The GluD2-Cbln1-neurexin system is thus critical for the formation and maintenance of the PF territory, and therefore should also contribute to the establishment of properly-segregated CF and PF territories.

Functional Implications. The transition from early exuberant innervation to mature topographical innervation has been elucidated for the neuromuscular junction, preganglionic projections to autonomic ganglion cells, CF-PC projections, retinogeniculate projections, thalamocortical projections to the sensory cortices, and endbulb and calyx synapses in the auditory brainstem pathway (3, 36–42). These types of synapses are refined through competition among homologous inputs, namely inputs that convey similar modalities of neural information from homonymous nuclei or sensory organs, but differ in their topography or laterality of projections.

Heterologous inputs from different nuclei or neural origins converge on given central neurons. They often innervate distinct dendritic domains, as exemplified by CF/PF inputs onto PCs, retinal/cortical inputs onto lateral geniculate relay neurons, and inputs from local/distant locations onto cortical pyramidal cells (3, 43, 44). This study provides a good example indicating that innervation by competing heterologous inputs is also refined through synapse elimination in cerebellar PCs. This refinement of PC synaptic wiring should influence information processing and integration at dendritic trees and the induction of heterosynaptic plasticity, both of which underlie cerebellar motor coordination and learning (45).

Materials and Methods

Animals. For each qualitative and quantitative analysis, we examined three C57BL6/J mice and three mutant mice deficient in mGluR1 (C57BL/6 background) (46) or PKCγ (hybrid background of C57BL/6 and 129/Ola) (47). All animal experiments received institutional approval, and were performed according to the guidelines for the care and use of laboratory animals of the Sapporo Medical University School of Medicine, Hiroshima University Graduate School of Biomedical & Health Sciences, The University of Tokyo Graduate School of Medicine, and Hokkaido University Graduate School of Medicine.

Immunofluorescence. Microslicer sections were prepared, and successively incubated at room temperature with 10% (vol/vol) normal donkey serum for 30 min, a mixture of primary antibodies overnight, and a mixture of species-specific secondary antibodies conjugated with FITC, Cy3, or Cy5 (1:200; Jackson ImmunoResearch) and Alexa Fluor 594-conjugated streptavidin (1:200; Invitrogen) to visualize BDA-labeled CFs. We used the following primary antibodies: rabbit anti-mGluR1α, rabbit and guinea pig anticalbindin, rabbit and goat anti-GFP, and goat anti-VGluT1. Rabbit anticalbindin antibody was diluted to 1:10,000, and other antibodies were used at the concentration of 1 μg/mL. Information on the sequence of antigens, host species, specificity, and references of each primary antibody is summarized in Table S1.

Images were taken with a confocal laser-scanning microscope (Radiance 2100, Zeiss) equipped with a Kry/Ar laser and a Plan-Apochromat (40×/1.0, 60×/1.4, 100×/1.4, oil immersion) objective lens (Zeiss). To avoid cross-talk between multiple fluorophores, Alexa594, FITC, and Cy5 fluorescent signals were acquired sequentially using the 488-, 568-, and 638-nm excitation laser lines, respectively. All images were acquired as single optical sections (512 × 512 pixels; pinhole size, 1.6 mm). For lentivius-mediated neuronal tracing, five consecutive optical sections were taken along the *z* axis at an interval of 1.0 μm to visualize the entire dendritic arbor (Fig. 3 *C* and *E*), and two sections at an interval of 1.0 μm were used for high-power imaging of proximal dendrites (Fig. 3 *D* and *F*).

Electron Microscopy. BDA-labeled CFs were visualized by overnight incubation with streptavidin-peroxidase conjugate (Nichirei) diluted with PB containing 0.5% Tween 20, followed by visualization using DAB. To identify PF and GABAergic synapses, sections were immunoreacted with goat anti-VGluT1 or anti-VIAAT antibody (1 μg/mL) overnight, respectively, and with 1.4-nm gold particle-conjugated anti-rabbit pig IgG (Nanogold, Nanoprobes) for 6 h. Sections were treated with the HQ silver kit (Nanoprobes), postfixed for 30 min with 1% osmium tetroxide in PB, block-stained overnight with 1% aqueous uranyl acetate solution, dehydrated using graded alcohols, and embedded in Epon 812. From the straight portion of lobules IV/V, three PCs were sampled at each stage for qualitative and quantitative analyses. Serial ultra-thin sections (100 nm in thickness) were cut in the plane parallel to the pial surface using an electron microscopy ultramicrotome (RMC-Boeckeler). A ribbon of more than 20 serial sections was mounted on each single-slot copper grid (1 × 2 mm) supported

with Formvar membrane. Electron micrographs were taken from every second section to cover the upper pole of PC somata to the distal most PF synapse using an H7650 electron microscope (Hitachi) at an original magnification of 15,000×. On each electron micrograph, the path length of curving and leaning dendrites was calculated (Fig. S4). Three-dimensional reconstruction was performed using the free software package Reconstruct, developed by Kristen Harris and John Fiala (available at Synapse Web: synapses.clm.utexas.edu/tools/reconstruct/reconstruct.stm).

Methods for tracer labeling, lentivirus experiment, and electrophysiology are described in *SI Materials and Methods*.

ACKNOWLEDGMENTS. We thank Prof. M. Yuzaki and Dr. K. Kohda (Keio University), and Dr. Uesaka (University of Tokyo) for the kind instruction on lentiviral experiments; and Mr. H. Okushima and Ms. E. Suzuki (Sapporo Medical University School of Medicine) for technical assistance. This study was supported by Grants-in-Aid for Scientific Research 24220007 (to M.W.), 17500233 and 24500413 (to R.I.), 25123716 and 25117006 (to K.H.), and 25000015 (to M.K.); the Strategic Research Program for Brain Sciences (Integrated Research on Neuropsychiatric Disorders (M.W. and K.H.); Development of Biomarker Candidates for Social Behavior (M.K.); and the Brain Mapping by Integrated Neurotechnologies for Disease Studies (Brain/MINDS) from Japan Agency for Medical Research and Development (AMED).

1. Crepel F, Delhaye-Bouchaud N, Dupont JL (1981) Fate of the multiple innervation of cerebellar Purkinje cells by climbing fibers in immature control, x-irradiated and hypothyroid rats. *Brain Res* 227(1):59–71.
2. Mariani J (1982) Extent of multiple innervation of Purkinje cells by climbing fibers in the olivocerebellar system of weaver, reeler, and staggerer mutant mice. *J Neurobiol* 13(2):119–126.
3. Watanabe M, Kano M (2011) Climbing fiber synapse elimination in cerebellar Purkinje cells. *Eur J Neurosci* 34(10):1697–1710.
4. Hashimoto K, Kano M (2003) Functional differentiation of multiple climbing fiber inputs during synapse elimination in the developing cerebellum. *Neuron* 38(5):785–796.
5. Kawamura Y, et al. (2013) Spike timing-dependent selective strengthening of single climbing fibre inputs to Purkinje cells during cerebellar development. *Nat Commun* 4:2732.
6. Hashimoto K, Ichikawa R, Kitamura K, Watanabe M, Kano M (2009) Translocation of a "winner" climbing fiber to the Purkinje cell dendrite and subsequent elimination of "losers" from the soma in developing cerebellum. *Neuron* 63(1):106–118.
7. Ichikawa R, et al. (2011) Developmental switching of perisomatic innervation from climbing fibers to basket cell fibers in cerebellar Purkinje cells. *J Neurosci* 31(47):16916–16927.
8. Carrillo J, Nishiyama N, Nishiyama H (2013) Dendritic translocation establishes the winner in cerebellar climbing fiber synapse elimination. *J Neurosci* 33(18):7641–7653.
9. Hashimoto K, et al. (2011) Postsynaptic P/Q-type Ca^{2+} channel in Purkinje cell mediates synaptic competition and elimination in developing cerebellum. *Proc Natl Acad Sci USA* 108(24):9987–9992.
10. Miyazaki T, Hashimoto K, Shin HS, Kano M, Watanabe M (2004) P/Q-type Ca^{2+} channel α1A regulates synaptic competition on developing cerebellar Purkinje cells. *J Neurosci* 24(7):1734–1743.
11. Miyazaki T, et al. (2012) Cav2.1 in cerebellar Purkinje cells regulates competitive excitatory synaptic wiring, cell survival, and cerebellar biochemical compartmentalization. *J Neurosci* 32(4):1311–1328.
12. Kano M, et al. (1995) Impaired synapse elimination during cerebellar development in PKC γ mutant mice. *Cell* 83(7):1223–1231.
13. Kano M, et al. (1997) Persistent multiple climbing fiber innervation of cerebellar Purkinje cells in mice lacking mGluR1. *Neuron* 18(1):71–79.
14. Levenes C, Daniel H, Jaillard D, Conquet F, Crépel F (1997) Incomplete regression of multiple climbing fibre innervation of cerebellar Purkinje cells in mGLuR1 mutant mice. *Neuroreport* 8(2):571–574.
15. Ichise T, et al. (2000) mGluR1 in cerebellar Purkinje cells essential for long-term depression, synapse elimination, and motor coordination. *Science* 288(5472):1832–1835.
16. Kakizawa S, Yamasaki M, Watanabe M, Kano M (2000) Critical period for activity-dependent synapse elimination in developing cerebellum. *J Neurosci* 20(13):4954–4961.
17. Hashimoto K, et al. (2001) Roles of glutamate receptor δ 2 subunit (GluRdelta 2) and metabotropic glutamate receptor subtype 1 (mGluR1) in climbing fiber synapse elimination during postnatal cerebellar development. *J Neurosci* 21(24):9701–9712.
18. Ichikawa R, et al. (2002) Distal extension of climbing fiber territory and multiple innervation caused by aberrant wiring to adjacent spiny branchlets in cerebellar Purkinje cells lacking glutamate receptor δ 2. *J Neurosci* 22(19):8487–8503.
19. Altman J (1972) Postnatal development of the cerebellar cortex in the rat. I. The external germinal layer and the transitional molecular layer. *J Comp Neurol* 145(3):353–397.
20. Hashimoto K, Kano M (2013) Synapse elimination in the developing cerebellum. *Cell Mol Life Sci* 70(24):4667–4680.
21. Miyazaki T, Fukaya M, Shimizu H, Watanabe M (2003) Subtype switching of vesicular glutamate transporters at parallel fibre-Purkinje cell synapses in developing mouse cerebellum. *Eur J Neurosci* 17(12):2563–2572.
22. Yamasaki M, Hashimoto K, Kano M (2006) Miniature synaptic events elicited by presynaptic Ca^{2+} rise are selectively suppressed by cannabinoid receptor activation in cerebellar Purkinje cells. *J Neurosci* 26(1):86–95.
23. Neale SA, Garthwaite J, Batchelor AM (2001) Metabotropic glutamate receptor subtypes modulating neurotransmission at parallel fibre-Purkinje cell synapses in rat cerebellum. *Neuropharmacology* 41(1):42–49.
24. Oberdick J, Smeyne RJ, Mann JR, Zackson S, Morgan JI (1990) A promoter that drives transgene expression in cerebellar Purkinje and retinal bipolar neurons. *Science* 248(4952):223–226.
25. Smeyne RJ, et al. (1991) Dynamic organization of developing Purkinje cells revealed by transgene expression. *Science* 254(5032):719–721.
26. Nakayama H, et al. (2012) GABAergic inhibition regulates developmental synapse elimination in the cerebellum. *Neuron* 74(2):384–396.
27. Finch EA, Augustine GJ (1998) Local calcium signalling by inositol-1,4,5-trisphosphate in Purkinje cell dendrites. *Nature* 396(6713):753–756.
28. Takechi H, Eilers J, Konnerth A (1998) A new class of synaptic response involving calcium release in dendritic spines. *Nature* 396(6713):757–760.
29. Dzubay JA, Otis TS (2002) Climbing fiber activation of metabotropic glutamate receptors on cerebellar Purkinje neurons. *Neuron* 36(6):1159–1167.
30. Hansel C, Linden DJ (2000) Long-term depression of the cerebellar climbing fiber—Purkinje neuron synapse. *Neuron* 26(2):473–482.
31. Kano M, Rexhausen U, Dreessen J, Konnerth A (1992) Synaptic excitation produces a long-lasting rebound potentiation of inhibitory synaptic signals in cerebellar Purkinje cells. *Nature* 356(6370):601–604.
32. Konnerth A, Dreessen J, Augustine GJ (1992) Brief dendritic calcium signals initiate long-lasting synaptic depression in cerebellar Purkinje cells. *Proc Natl Acad Sci USA* 89(15):7051–7055.
33. Regehr WG, Mintz IM (1994) Participation of multiple calcium channel types in transmission at single climbing fiber to Purkinje cell synapses. *Neuron* 12(3):605–613.
34. Matsuda K, et al. (2010) Cbln1 is a ligand for an orphan glutamate receptor δ2, a bidirectional synapse organizer. *Science* 328(5976):363–368.
35. Uemura T, et al. (2010) Trans-synaptic interaction of GluRdelta2 and Neurexin through Cbln1 mediates synapse formation in the cerebellum. *Cell* 141(6):1068–1079.
36. Lichtman JW, Colman H (2000) Synapse elimination and indelible memory. *Neuron* 25(2):269–278.
37. Iwasato T, et al. (2000) Cortex-restricted disruption of NMDAR1 impairs neuronal patterns in the barrel cortex. *Nature* 406(6797):726–731.
38. Hensch TK (2005) Critical period plasticity in local cortical circuits. *Nat Rev Neurosci* 6(11):877–888.
39. Lu T, Trussell LO (2007) Development and elimination of endbulb synapses in the chick cochlear nucleus. *J Neurosci* 27(4):808–817.
40. Stevens B, et al. (2007) The classical complement cascade mediates CNS synapse elimination. *Cell* 131(6):1164–1178.
41. Holcomb PS, et al. (2013) Synaptic inputs compete during rapid formation of the calyx of Held: A new model system for neural development. *J Neurosci* 33(32):12954–12969.
42. Lichtman JW, Purves D (1980) The elimination of redundant preganglionic innervation to hamster sympathetic ganglion cells in early post-natal life. *J Physiol* 301:213–228.
43. Sherman SM, Guillery RW (2004) Thalamus. *The Synaptic Organization of the Brain*, ed Shepherd GM (Oxford Univ, New York), pp 311–359.
44. Spruston N (2008) Pyramidal neurons: Dendritic structure and synaptic integration. *Nat Rev Neurosci* 9(3):206–221.
45. Ito M (2012) *Cerebellum: The Brain for an Implicit Self* (Pearson Education, Inc., publishing as FT Press, Upper Saddle River, NJ).
46. Aiba A, et al. (1994) Reduced hippocampal long-term potentiation and context-specific deficit in associative learning in mGluR1 mutant mice. *Cell* 79(2):365–375.
47. Abeliovich A, et al. (1993) Modified hippocampal long-term potentiation in PKC γ-mutant mice. *Cell* 75(7):1253–1262.
48. Hanawa H, et al. (2004) Efficient gene transfer into rhesus repopulating hematopoietic stem cells using a simian immunodeficiency virus-based lentiviral vector system. *Blood* 103(11):4062–4069.
49. Sawada Y, et al. (2010) High transgene expression by lentiviral vectors causes maldevelopment of Purkinje cells in vivo. *Cerebellum* 9(3):291–302.
50. Maejima T, Hashimoto K, Yoshida T, Aiba A, Kano M (2001) Presynaptic inhibition caused by retrograde signal from metabotropic glutamate to cannabinoid receptors. *Neuron* 31(3):463–475.
51. Nakagawa S, Watanabe M, Isobe T, Kondo H, Inoue Y (1998) Cytological compartmentalization in the staggerer cerebellum, as revealed by calbindin immunohistochemistry for Purkinje cells. *J Comp Neurol* 395(1):112–120.
52. Miura E, et al. (2006) Expression and distribution of JNK/SAPK-associated scaffold protein JSAP1 in developing and adult mouse brain. *J Neurochem* 97(5):1431–1446.
53. Takasaki C, et al. (2010) Cytochemical and cytological properties of perineuronal oligodendrocytes in the mouse cortex. *Eur J Neurosci* 32(8):1326–1336.
54. Tanaka J, et al. (2000) Gq protein alpha subunits Galphaq and Galpha11 are localized at postsynaptic extra-junctional membrane of cerebellar Purkinje cells and hippocampal pyramidal cells. *Eur J Neurosci* 12(3):781–792.